University of Bath

Kinetics of Asymmetric Transfer Hydrogenation, Catalyst Deactivation, and Inhibition with Noyori Complexes As Revealed by Real-Time High-Resolution FlowNMR Spectroscopy

Andrew M. R. Hall,[†,‡] Peilong Dong,[§] Anna Codina,[∥] John P. Lowe,[‡,§] and Ulrich Hintermair*,[†,‡]

†Centre for Sustainable Chemical Technologies, ‡Dynamic Reaction Monitoring Facility, and §Department of Chemistry, University of Bath, Bath BA2 7AY, United Kingdom

∥Bruker UK, Banner Lane, Coventry CV4 9GH, United Kingdom

S Supporting Information

ABSTRACT: Catalytic hydrogen transfer from basic isopropyl alcohol to aryl ketones mediated by [(arene)-(TsDPEN)RuCl] complexes has been investigated by operando ^1H NMR spectroscopy using a recirculating flow setup. Selective excitation pulse sequences allowed fast and quantitative monitoring of the key [(mesitylene)(TsDPEN)-RuH] intermediate during catalysis, which is shown to interact with both substrates by polarization transfer experiments. Comparison of reaction profiles with catalyst speciation traces in conjunction with reaction progress kinetic analysis using variable time normalization and kinetic modeling showed the existence of two independent catalyst deactivation/inhibition pathways: whereas excess base exerted a competitive inhibition effect on the unsaturated catalyst intermediate, the active hydride suffered from an inherent first-order decay that is not evident in early stages of the reaction where turnover is fast. Isotopic labeling revealed arene loss to be the entry point into deactivation pathways to Ru nanoparticles via hydride-bridged intermediates.

KEYWORDS: reaction monitoring, NMR spectroscopy, transition metal catalysis, kinetics, transfer hydrogenation
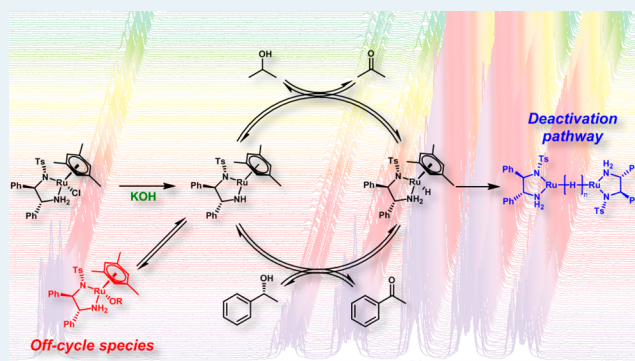
INTRODUCTION

Homogeneous catalysis is an extremely powerful tool for chemical synthesis, offering molecular engineering of complex transformations with unrivaled precision under mild conditions.[1−3] Understanding the reactivity displayed by the catalyst, including possible inhibition and deactivation pathways,[4] is key to improving existing systems and developing new catalytic technologies.[5−7] Due to the complex and dynamic nature of catalytic systems operating under kinetic control, this is still a significant challenge. Reaction progress monitoring and kinetic analysis can guide catalyst development but require high-quality data and do not provide information on the identity and structure of the various intermediates and off-cycle species inferred.[8−12] *Operando* methods that allow the kinetics of the reaction to be measured and the speciation of the catalyst to be observed under realistic conditions are thus key to advancing catalysis research.[13] Online or in situ techniques such as UV−vis, infrared (IR), and Raman spectroscopies, along with sampling gas chromatography (GC), mass spectrometry (MS), or high-performance liquid chromatography (HPLC) are often used for reaction monitoring and analysis[14−19] and can be very powerful for selected analytes. However, most of these techniques require calibration before use and are not amenable to noninvasive observation of a priori unknown catalytic intermediates. Multinuclear high-resolution FlowNMR spectroscopy has recently emerged as a powerful tool for real-time reaction monitoring,[20−26] providing a wealth of information about complex mixtures and overcoming many of the limitations of alternative in situ and off-line techniques due to the ability to maintain realistic reaction conditions, including good mass transport and temperature control (Figure 1). As long as residence time and flow effects on signal quantification are considered, highly accurate data may be obtained without any modification of the NMR spectrometer.[20,21,24,27]

Transition-metal-catalyzed asymmetric transfer hydrogenation reactions are an important synthetic procedure commonly used to introduce chirality into a molecule through reduction of prochiral ketones or imines to alcohols and amines with high enantioselectivities.[28−36] One of the earliest examples and still most powerful catalyst systems are Noyori's original TsDPEN complexes which contain a chiral diamine ligand bound to a ruthenium center.[37,38] These combine exquisite chemoselectivities, high reaction rates, and excellent stereoselectivities for a range of aryl ketones, work with both isopropyl alcohol and
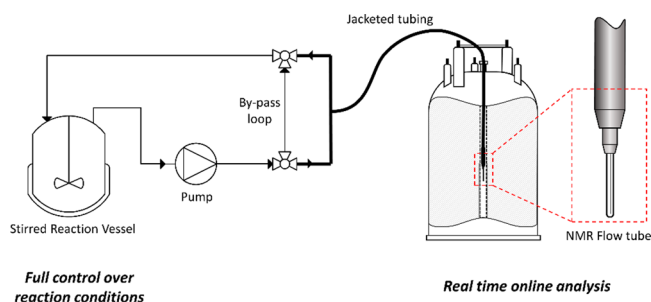
Figure 1. FlowNMR apparatus schematic (not to scale).

formic acid as the reductant, and tolerate a range of auxiliary bases.[39,40] Despite their effectiveness and ease of use, however, turnover numbers are still limited due to catalyst deactivation.[4] A lot of effort has been devoted to understanding the mechanism of hydrogen transfer,[31,38,40−44] but little is known about the origin and nature of catalyst deactivation in these systems.

Here, we investigate the asymmetric transfer hydrogenation of acetophenone with Noyori's [(mesitylene)((R,R)-TsDPEN)-RuCl] catalyst (Scheme 1) using real-time FlowNMR spectros-

Scheme 1. Catalytic Asymmetric Transfer Hydrogenation of Acetophenone to (R)-1-Phenylethanol with RuCl[(R,R)-TsDPEN](mesitylene) (1)
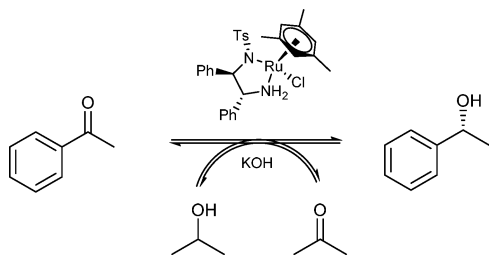

copy to readily obtain high-quality kinetic data on this air-sensitive, transition-metal-catalyzed transformation. We find that no modification of the reaction conditions is required, and a wealth of highly accurate and precise data is generated with a minimum amount of reagents and experimental time. Using selective excitation pulse sequences, we were able to follow the catalyst speciation under turnover conditions at the same time, information that in conjunction with kinetic analysis and strategic isotope labeling leads to the formulation of an expanded mechanism for this widely used reaction that includes and explains inhibition and deactivation pathways.

RESULTS AND DISCUSSION

We found that no modification of the reaction conditions (scale, concentrations, solvent, reaction vessel, etc.) was required for the analysis by FlowNMR; all experiments discussed in the following were performed under literature conditions ($V = 10$ mL, 0.4 M substrate, 0.25−1 mol % of [Ru], 1−20 equiv of KOH, inert atmosphere, room temperature, isopropyl alcohol-H_8). For a 10 mL reaction volume, the sample spends approximately 37% of the reaction time within the flow apparatus ($V = 3.7$ mL).[20] The volume of the NMR flow cell used was approximately 0.5 mL, corresponding to a mean residence time within the detection region of 8 s at a typical flow rate of 4 mL min^{-1}. As described earlier,[20] the high field and shim stability of modern spectrometers together with application of advanced multiple solvent suppression techniques

allowed the use of nondeuterated solvents, which is particularly important in cases like transfer hydrogenation, where deuterated solvents would otherwise lead to unwanted isotope effects (as demonstrated further below). Like its many variations, the original Noyori catalyst is known to be air-sensitive in solution, gradually decomposing to Ru nanoparticles[45,46] that progressively erode reaction rates and stereoselectivity (Table S1). Thus, all reagents and solvents were dried and degassed, and the FlowNMR apparatus (consisting mainly of HPLC grade PEEK and Teflon tubing) was purged with argon and flushed with dry solvent prior to use. The reactions were carried out in a standard Schlenk-type glass flask with magnetic stirring under dry argon atmosphere, with the sample tubing to and from the FlowNMR tube fed through a rubber seal. At typical flow rates of 4 mL/min, residence times in the apparatus were about 1 min, resulting in a 30 s time lapse between the reaction vessel and NMR detection. Continuous NMR spectra acquisition was set up and started on a flow of solvent, and the reaction was initiated by sequential addition of reagents via airtight syringes.

With this setup (Figure 1) and using optimized ^{1}H NMR acquisition parameters accounting for flow effects[20] (for details, see Supporting Information), we were able to follow catalytic product formation in real time, providing high-quality kinetic reaction profiles (Figure 2). The solution of the flow experiment
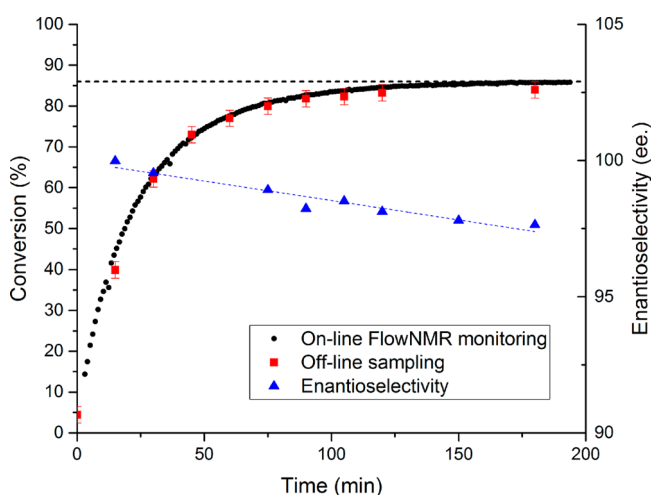
Figure 2. Reaction progress and enantioselectivity data for the catalytic transfer hydrogenation of acetophenone to (R)-1-phenylethanol (400 mM acetophenone, 10 mM KOH, 2 mM **1**, 9.5 mL of dry isopropyl alcohol, 20 °C) monitored using online ^{1}H FlowNMR spectroscopy and off-line ^{1}H NMR spectroscopy on samples taken from the reaction mixture at different time points throughout the reaction. Off-line reaction was performed in a sealed Schlenk flask under inert atmosphere. Online FlowNMR reaction was performed in a sealed round-bottom flask under inert conditions (see Supporting Information for details). Enantioselectivity determined by chiral HPLC analysis (see Supporting Information for details).

went through the same color changes over time as a separate control experiment in a sealed Schlenk flask, and comparing conversions and enantioselectivities over time as derived from the FlowNMR experiment with data from off-line sampling showed identical values (Figure 2).

The reaction profile smoothly converged to equilibrium (86 ± 2% conversion under the conditions applied) over the course of a few hours, with no noticeable induction period once the catalyst precursor **1** was added to a solution of acetophenone

and KOH in deaerated isopropyl alcohol. Enantioselectivity toward (R)-1-phenylethanol was >99% ee up to about 50% conversion, then started to decrease to 98% ee near equilibrium conversion and continued to fall when the reaction was left for longer. This behavior is known and typically ascribed to the reversibility of the reaction,[35] but catalyst deactivation to less selective species also contributes to the erosion of enantioselectivity over time (Figure 2).

The quantitative nature and high quality of the reaction profiles obtained makes the data well-suited for reaction progress kinetic analysis (RPKA).[8] Variable time normalization analysis (VTNA) has recently been shown to be particularly useful for performing RPKA directly on integral rate data such as derived from spectroscopy.[9,47] Applying variable time normalization to reaction profiles obtained with different amounts of **1** showed good overlay when plotted against $\{time \times [cat]^n\}$ with $n = 1.0$, revealing a first-order rate dependence on ruthenium concentration (Figure 3). The same method, plotting $\{time \times [acetophenone]^n\}$ also revealed a first-order dependence in substrate (Figure S1). This reaction order is in agreement with that derived from initial rate data (Figure S2) and with the proposed mechanism involving monomeric ruthenium species in the turnover-limiting step (TLS).[48,49] However, although the overlay is very good in the initial regime of the reaction up to ~50% conversion and identical equilibrium conversions were reached at longer reaction times, lower normalized rates were evident for lower catalyst loadings at intermediate reaction stages (Figure 3, inset), indicating some catalyst deactivation over the course of the reaction.

The reverse reaction starting with acetone and racemic 1-phenylethanol resulted in a conversion of 16% of the (R)-1-phenylethanol to acetophenone with negligible conversion of (S)-1-phenylethanol (Figure 4a), confirming the reversibility of
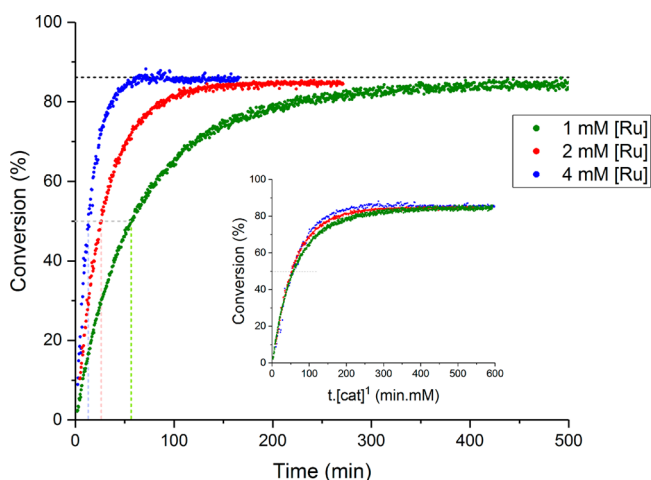
Figure 3. Conversion plots for the catalytic transfer hydrogenation of acetophenone to (R)-1-phenylethanol with various amounts of **1** (400 mM acetophenone, 10 mM KOH, 9.5 mL of dry isopropyl alcohol, 20 °C), showing dependence of catalyst concentration on reaction rate. Inset: VTNA of conversion data.

the reaction and the final conversion values seen in the forward reaction to be equilibrium under the conditions applied. Injection of a second portion of substrate showed the catalyst to remain active after the initial end-point had been reached, albeit with only about half the initial reaction rate and reduced enantioselectivity (Figure 4b).

The ability to readily acquire high-quality reaction profiles suitable for kinetic analyses without prior calibration makes FlowNMR an attractive tool for reaction development and optimization.[21,23] For mechanistic investigations in catalysis, however, it would be even more desirable to also follow catalyst speciation at the same time, because, if intermediates can be observed under the same conditions as product formation takes place, we can understand their kinetic relevance, a crucial link that is missing from traditional ex situ analyses and model reactions.[13] We thus strived to detect catalyst intermediates during acetophenone reduction from isopropyl alcohol catalyzed by **1** directly under the standard literature conditions used.

Akin to related olefin reduction, the traditional Meerwein–Ponndorf–Verley mechanism for ketone reduction involves direct (i.e., inner-sphere) coordination of the substrates to the metal, from which the alkoxide product is liberated after hydride addition to the activated carbonyl.[31,41] An alternative mechanism explaining the very high chemoselectivities of C=O versus C=C reduction observed with ruthenium diamine complexes involves an outer-sphere pathway, where hydrogen atoms are transferred from a metal hydride and amine proton in a metal–ligand bifunctional manner (HOL/TOL mechanisms in Morris' classification[41]) that does not require the substrates to coordinate to the metal.[31,35,38,39] As shown by Noyori, treatment of the precursor complex **1** with a base such as potassium hydroxide leads to deprotonation of the bound amine and loss of the chloride ligand, resulting in the "unsaturated" 16 electron complex **2** (Scheme 2). Addition of a reducing alcohol to **2** then results in the formation of the 18 electron monohydride complex **3** along with the corresponding ketone. **3** may transfer the reducing equivalents to another ketone, leading to re-formation of **2** and the corresponding alcohol (with stereocontrol in this case).

It is important to note that although various versions of this mechanism based on different transition states have been discussed,[48] the involvement of **2** and **3** as the key catalytic intermediates is common to all these scenarios.[49] Thus, our following mechanistic discussion is based on **2** and **3** as the main in-cycle species, and we refrain from speculating on *how* these interconvert during turnover in this paper.
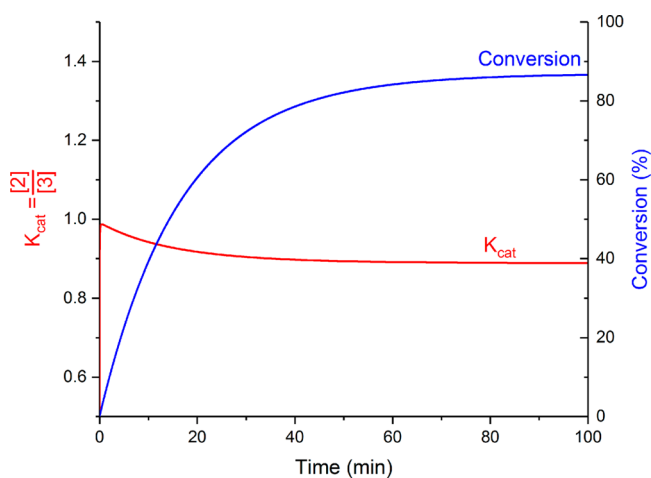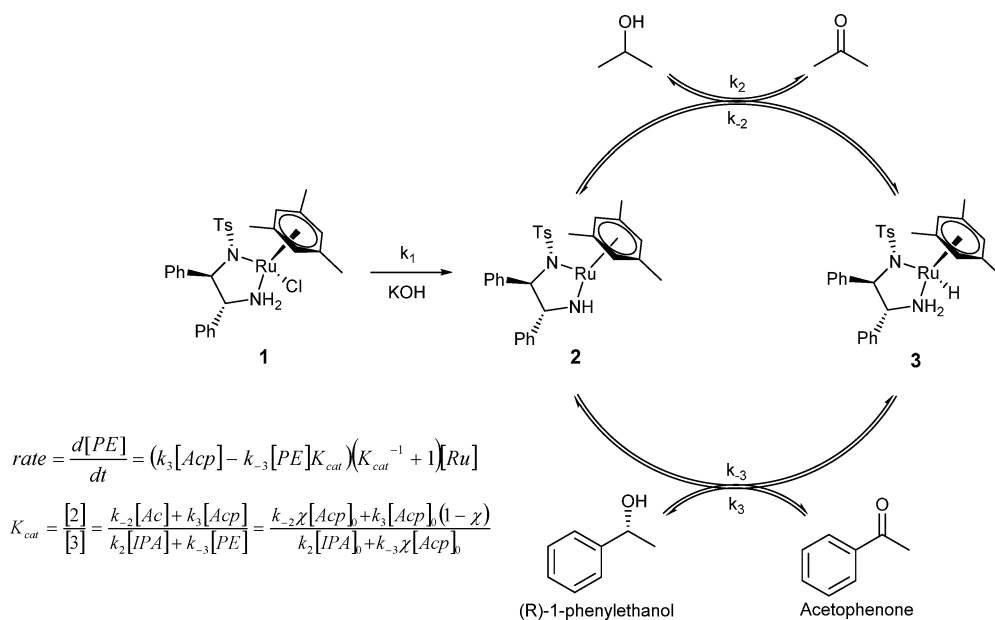
Because all in-cycle events are fully reversible when using isopropyl alcohol as the reductant, the rate law for this simple mechanism contains four rate constants, and the distribution of catalyst during turnover expressed as $K_{cat} = \frac{[2]}{[3]}$ is a function of all of these as well as the reaction progress χ (Scheme 2). Kinetic modeling of the catalyst speciation over the course of the reaction (see Supporting Information for details) shows an initial 1:1 distribution between **2** and **3**, which asymptotically falls to $K_{cat} = \frac{[2]}{[3]} = 0.88$ over the course of the reaction under the conditions applied (Figure 5). The fact that K_{cat} is predicted not to change further once final conversion values have been reached reflects the reversibility of the reaction and shows the catalyst to remain busy cycling in the equilibrium mixture.

The reduced catalyst intermediate **3** contains a ruthenium monohydride that is characterized by a singlet peak reported at −5.47 ppm (toluene-d_8) in the ^1H NMR spectrum,[38] which presents itself as a convenient spectroscopic handle as no other component of the reaction mixture has any resonances in this chemical shift range. However, the low concentration of catalyst (0.25−1 mol % relative to substrate) means that under catalytic
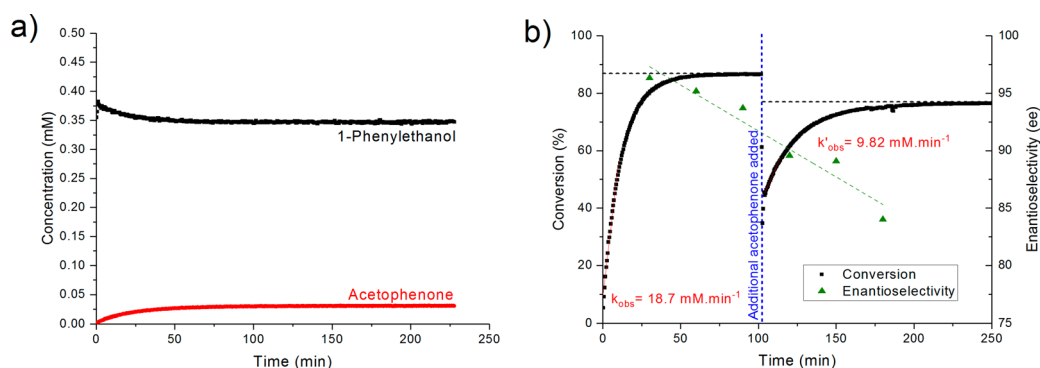
Figure 4. (a) Reaction profiles for the transfer hydrogenation of racemic 1-phenylethanol and acetone to acetophenone and isopropyl alcohol (400 mM *rac*-1-phenylethanol, 10 mM KOH, 9.5 mL of dry acetone, 2 mM **1**, 20 °C). (b) Reaction profiles and enantioselectivity for the catalytic transfer hydrogenation of acetophenone to (*R*)-1-phenylethanol (400 mM acetophenone, 10 mM KOH, 4 mM **1**, 9.5 mL of dry isopropyl alcohol, 20 °C) where an additional 4 mmol acetophenone was added after 100 min (800 mM total acetophenone concentration).

Scheme 2. Commonly Accepted Mechanism of the Catalytic Asymmetric Transfer Hydrogenation of Acetophenone Using RuCl[(*R,R*)-TsDPEN](mesitylene) (1) in Basic Isopropyl Alcohol and Its Corresponding Rate Law

$$rate = \frac{d[PE]}{dt} = \left(k_3[Acp] - k_{-3}[PE]K_{cat}\right)\left(K_{cat}^{-1} + 1\right)[Ru]$$

$$K_{cat} = \frac{[2]}{[3]} = \frac{k_{-2}[Ac] + k_3[Acp]}{k_2[IPA] + k_{-3}[PE]} = \frac{k_{-2}\chi[Acp]_0 + k_3[Acp]_0(1-\chi)}{k_2[IPA]_0 + k_{-3}\chi[Acp]_0}$$

Figure 5. Simulation of the change in K_{cat} and conversion during course of reaction (see Supporting Information for details of simulation, kinetic parameters, and derivation of rate laws).

conditions, where only a part of the ruthenium exists as **3**, the hydride peak is within the noise level of the ^{1}H NMR spectrum at 500 MHz (Figure 6) because the receiver gain of the instrument is limited by the much larger solvent and substrate signals. Use of a shaped excitation pulse sequence (see Supporting Information for details), however, enabled the hydride region of the spectrum to be amplified selectively, with minimal excitation of off-resonance peaks. This allowed the receiver gain to be adjusted to increase the signal-to-noise ratio (S/N) for the hydride peak of **3**, effectively amplifying its signal by >1000 times (Figure 6). Although no significant change in line width was detectable throughout the reaction at room temperature, polarization transfer experiments (EXSY NMR) of **3** thus observed under reaction conditions showed a (on the NMR time scale) fast exchange between the ruthenium hydride and both the isopropyl alcohol and 1-phenylethanol CH protons (Figure S3). These data are direct proof for **3** to be an in-cycle catalytic species undergoing continuous reversible exchange with both substrate and product (Scheme 2), and represents key information for mechanistic interpretation of the intermediate
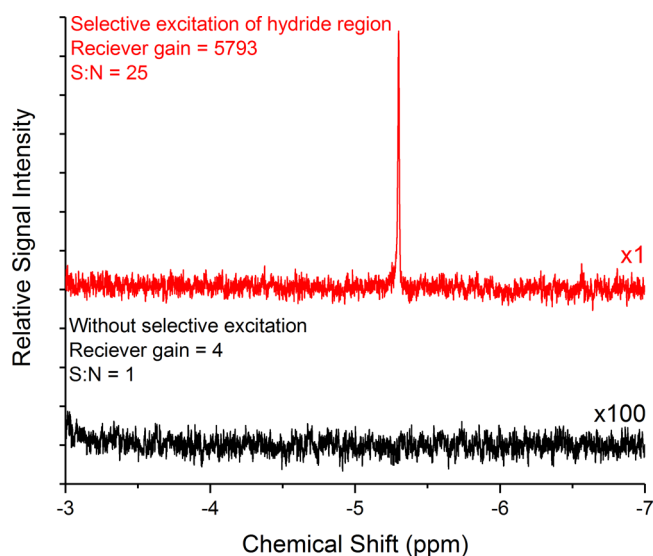
Figure 6. Selective ^{1}H excitation of the hydride peak of **3** under turnover conditions in flow (4 mL/min) using a gradient spin echo pulse sequence with a shaped 180° pulse centered at −5.4 ppm, resulting in >1000 times increase in signal amplification (without selective excitation: 4 scans, 1 s acquisition time, 4 s delay time; selective excitation: 24 scans, 1 s acquisition time, 1 s delay time, 880 μs Gaussian-shaped pulse; both spectra processed with 0.5 Hz exponential line broadening). Data for experiment without selective excitation multiplied by a factor of 100 for visual clarity.

observed that would be very difficult to obtain using other reaction monitoring techniques.

A selectively excited ^{1}H spectrum with good S/N could be acquired in less than 1 min and was found to be fully compatible with continuous flow conditions. The spectrometer used (see Supporting Information for details) exhibited a linear signal response with increasing receiver gain, allowing for quantitative
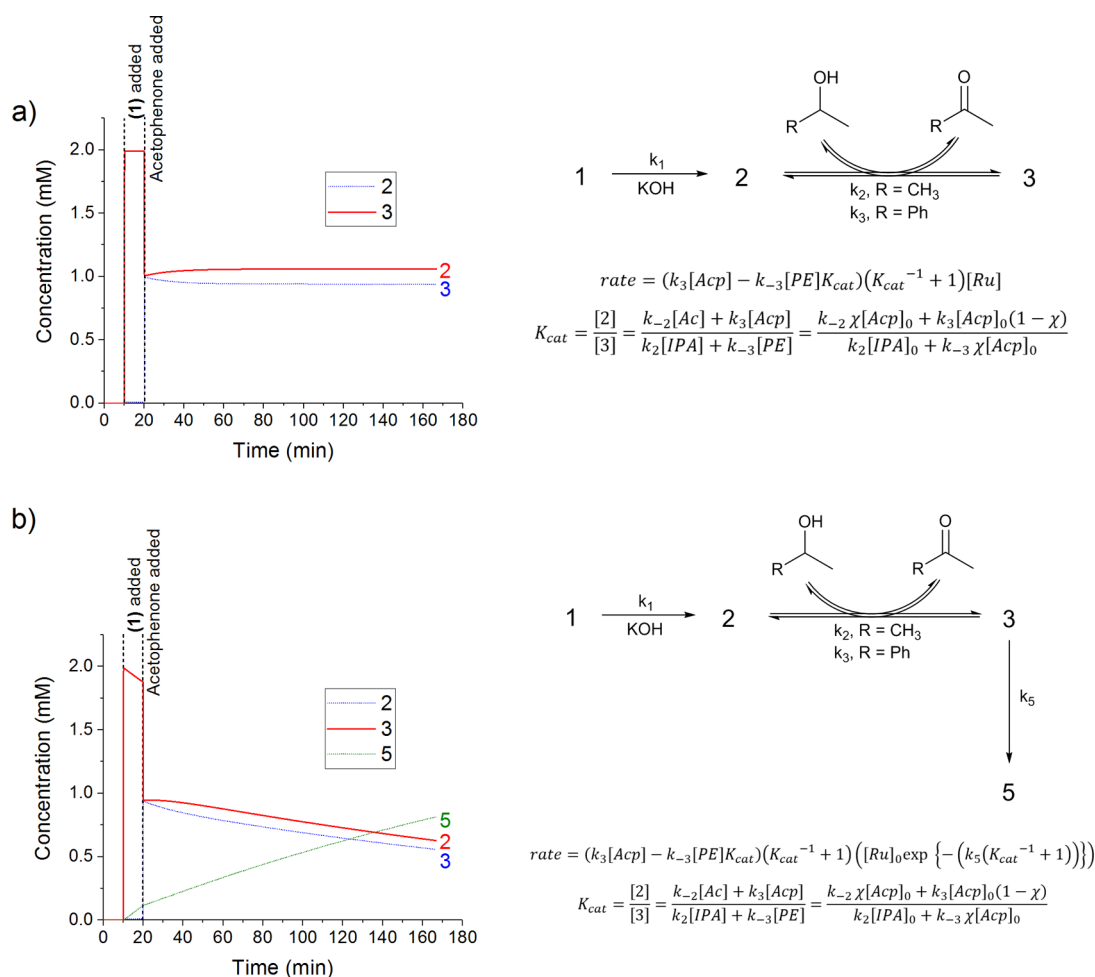
integration of the selectively excited peak (Figure S9). Thus, interleaving normal +10 to 0 ppm ^{1}H scans with selectively excited 0 to −10 ppm ^{1}H scans allowed us to track both the reaction progress as well the catalyst speciation under the same conditions in a single ^{1}H FlowNMR experiment, all while giving the operator full control over the reaction conditions.

The versatility and power of this setup is demonstrated in the experiment shown in Figure 7, from which a wealth of information can be derived. Addition of **1** to the reaction vessel containing a stirred solution of KOH in isopropyl alcohol-H$_8$ led to the rapid formation of a peak at −5.3 ppm indicative of **3**. This showed the activation of the precursor **1** to be fast and quantitative under the conditions applied, in line with the absence of any noticeable induction periods in the conversion profiles (Figure 2). As no substrate was present at this point, the catalyst resided exclusively in the reduced hydride form, however, with some noticeable decrease in concentration over time (discussed below). Addition of acetophenone substrate (0.47 mL, 4 mmol) caused the concentration of the hydride complex **3** to drop to 54% of the concentration prior to substrate addition, indicating catalytic turnover taking place that involves cycling of the catalyst through the unsaturated intermediate **2** to give an experimentally determined K_{cat} = 0.85 close to the predicted value of 0.88 (Figure 5).

The concentration of **3** remained steady during the initial stages of the reaction up to 50% conversion, after which another, slower decrease in concentration set in over the later stage of the reaction which was not predicted by the kinetic modeling of the simple mechanism (Figure 5). This correlated exactly with the deviation seen in the VTNA of the reaction progress profiles (Figure 3) and further indicated catalyst deactivation, consistent with the reduced reaction rates observed upon catalyst reuse (Figure 4b). Visual observation of gradual darkening of the reaction mixture over time suggested the eventual formation of Ru black (Figure S4), a transformation that was faster and more pronounced when the reaction was performed in air (Table S1),
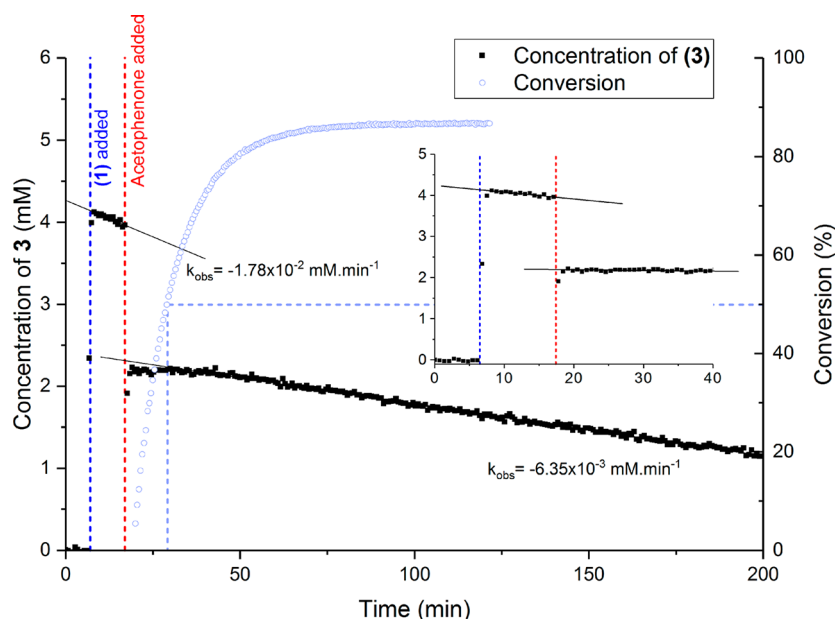
Figure 7. Concentration profile of the hydride peak of **3** at −5.3 ppm and conversion profile of acetophenone to (R)-1-phenylethanol, during the course of catalytic transfer hydrogenation of acetophenone to (R)-1-phenylethanol in flow at 4 mL/min (400 mM acetophenone, 10 mM KOH, 4 mM **1**, 9.5 mL of dry isopropyl alcohol, 20 °C). Selective excitation of **3** using a gradient spin echo pulse sequence with a shaped 180° pulse centered at −5.3 ppm (8 scans, 2 s acquisition time, 1 s delay time, 1600 μs Gaussian-shaped pulse).

$$rate = (k_3[Acp] - k_{-3}[PE]K_{cat})(K_{cat}^{-1} + 1)[Ru]$$

$$K_{cat} = \frac{[2]}{[3]} = \frac{k_{-2}[Ac] + k_3[Acp]}{k_2[IPA] + k_{-3}[PE]} = \frac{k_{-2}\chi[Acp]_0 + k_3[Acp]_0(1 - \chi)}{k_2[IPA]_0 + k_{-3}\chi[Acp]_0}$$

$$rate = (k_3[Acp] - k_{-3}[PE]K_{cat})(K_{cat}^{-1} + 1)\left([Ru]_0 \exp\left\{-\left(k_5(K_{cat}^{-1} + 1)\right)\right\}\right)$$

$$K_{cat} = \frac{[2]}{[3]} = \frac{k_{-2}[Ac] + k_3[Acp]}{k_2[IPA] + k_{-3}[PE]} = \frac{k_{-2}\chi[Acp]_0 + k_3[Acp]_0(1 - \chi)}{k_2[IPA]_0 + k_{-3}\chi[Acp]_0}$$

Figure 8. Simulated catalyst distribution profiles for (a) conventional mechanism of catalytic transfer hydrogenation of acetophenone considering only active intermediates **2** and **3** and (b) with inclusion of irreversible catalyst deactivation from **3**. See Supporting Information for details of simulation, kinetic parameters, and derivation of rate laws.
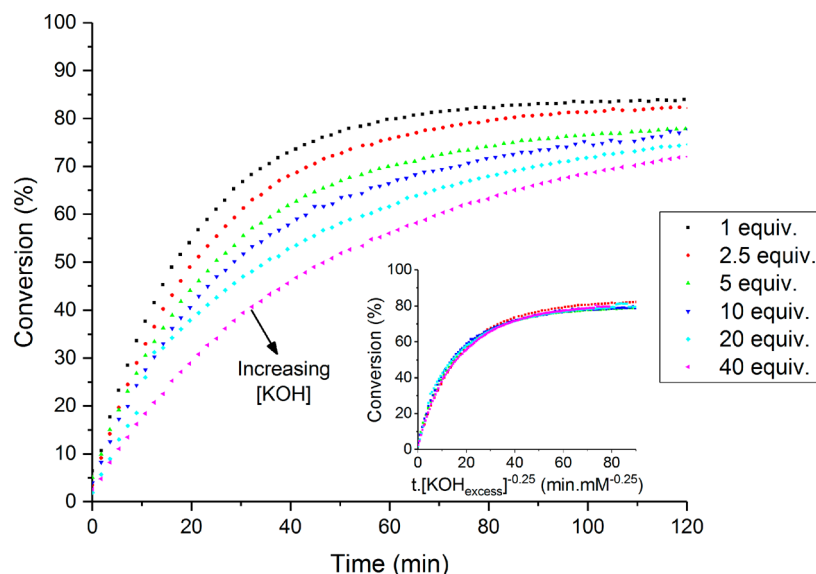
Figure 9. Conversion plots for the catalytic transfer hydrogenation of acetophenone to (*R*)-1-phenylethanol (400 mM acetophenone, 2 mM **1**, 9.5 mL of dry isopropyl alcohol, 20 °C) with varying equivalents of KOH per [Ru] (1 scan, 1.64 s acquisition time, 1 s relaxation delay time). Inset: VTNA plot of conversion data, indicating a −0.25 order in excess KOH on reaction rate.

consistent with the known oxygen sensitivity of the activated catalyst.[45,46]

The rate of catalyst deactivation being greatest before the addition of acetophenone substrate (Figure 7, inset) suggests

the process to occur directly from the hydride intermediate **3**, which is the dominant ruthenium species prior to the system entering turnover. Upon taking up substrate turnover, the rate of deactivation is decreased, as a smaller percentage of catalyst is present in the hydride form, which quickly interconverts to **2** and back. The conventional TOL mechanism[41] shown in Scheme 2 does not account for catalyst deactivation, and kinetic modeling of the concentration of **3** over the course of the reaction showed that none of the decreases in the concentration of **3** observed experimentally are described by its rate law (Figure 8a). Introduction of a (relatively) slow, irreversible catalyst deactivation pathway producing an inactive species **5** from **3** introduces a deactivation term to the rate law that decreases the amount of ruthenium available to productively cycle between **2** and **3**. Kinetic modeling of this expanded rate law reproduced the experimentally observed catalyst profile both before and after substrate addition (Figure 8b).

The auxiliary base, KOH in this case, is another important part of the catalyst system that is known to affect its performance.[41] In metal−ligand bifunctional transfer hydrogenation catalysis, the external base is thought not to be involved in any in-cycle transformations,[38,49] so in theory 1 equivalent per ruthenium suffices to initiate the catalysis. In practice, however, various amounts of excess base are used to ensure fast and complete precursor activation.[35,37,38] As noted by others before,[50] we found that increasing base concentration also led to a decrease in the rate of product formation (Figure 9), with VTNA revealing an order of −1/4 for the influence of excess KOH. [As hydroxide (pK_a 15.7) and isopropoxide (pK_a 16.5) are in equilibrium in solution this value may not easily be interpreted directly].

This observation alone might suggest the involvement of KOH in the catalyst deactivation discussed above; however, monitoring the concentration of **3** during reactions with various amounts of excess base showed the rate of catalyst deactivation, as indicated by the slope of the decay of **3** over time, to be *independent* of base concentration (Figure 10). Instead, increasing base concentration led to a decrease in the amount of hydride present during turnover. (As shown by the rate law, a base-induced shift in K_{cat} would not lead to decreased product formation rates.) The fact that prior to entering catalysis the same amount of **3** is generated in all cases, with similar decreases due to progressive formation of **5**, strongly suggests a second, independent inhibition mechanism caused by the action of excess base on **2**.

These data therefore revealed the existence of another off-cycle ruthenium species **4** that further reduces the concentration of active ruthenium available to the catalytic cycle, causing the apparent decrease in concentration of **3** via consumption of **2**, thereby leading to the observed reduction in turnover rate (Scheme 3). Indeed, a classical Lineweaver−Burk analysis of reaction rates at different base loadings showed excess base to exert competitive inhibition behavior on product formation (Figure S5). A further expansion of the mechanism and associated rate law including off-cycle species **4** formed by reaction of **2** with base (either hydroxide or isopropoxide) enabled our kinetic model to accurately reproduce the effects of increasing base on both the product formation kinetics as well as the hydride concentration profiles (Figure 11). Without inclusion of **4**, there is no difference between the simulated kinetic profiles at different base concentrations. Combining catalyst inhibition by formation of **4** from **2** and catalyst deactivation by formation of **5** from **3** yields the modified reaction mechanism shown in Scheme 3, which accounts for all
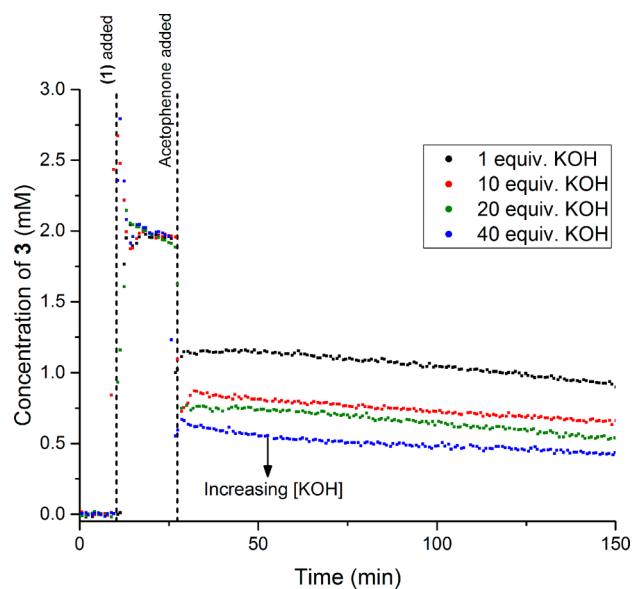
Figure 10. Concentration profiles of the hydride peak of **3** at −5.3 ppm during the course of catalytic transfer hydrogenation of acetophenone to (*R*)-1-phenylethanol in flow at 4 mL/min (400 mM acetophenone, 2 mM **1**, 9.5 mL of dry isopropyl alcohol, 20 °C) with varying equivalents of KOH per [Ru]. Selective excitation of **3** using a gradient spin echo pulse sequence with a shaped 180° pulse centered on the hydride peak (8 scans, 2 s acquisition time, 1 s delay time, 1600 μs Gaussian-shaped pulse).

experimental observations describing both the reaction progress as well as catalyst speciation by its associated rate law.

Once the various catalyst deactivation phenomena have been quantitatively identified, they can be factored into the RPKA analysis to check whether they now accurately describe the kinetic behavior of the system over the course of the reaction.[9,47] Including the deactivation rates from our expanded rate law (Scheme 3) in the VTNA of the reaction progress at different ruthenium loadings (Figure 3) indeed produced excellent overlay across the entire profile (Figure 12). The model also accurately reproduces the reaction progress at different substrate concentrations as well as Ru−H profiles and enantioselectivity over time (Figures S11−S14).

The final piece of information required to improve the catalysis is understanding the molecular origin of the deactivation/inhibition events identified. In this case, based on the kinetic evidence of competitive base inhibition, off-cycle species **4** are most likely simple base adducts of **2** (Scheme 4). Indeed, an earlier computational study by Noyori et al. proposed the reversible formation of stable alkoxide complexes by reaction of **2** with alcohols or other protic compounds potentially acting as off-cycle reservoirs of **2** in the catalytic cycle.[49] Similarly, the related formate adducts are known and have been shown to inhibit transfer hydrogenation catalysis from formic acid/triethylamine mixtures.[43,44] Thus, although the structures of **4** are currently not known with certainty (all of our attempts at detecting or isolating various base adducts of **1** or **2** have failed so far, and no structurally characterized examples have been reported in the literature either), the fact their formation may be limited simply by using a minimum amount of base (i.e., stoichiometric in **1**) together with the observation that any excess base (if present) does not contribute to other deactivation phenomena during the course of the reaction is sufficient information for optimal use of **1** with regards to the amount of
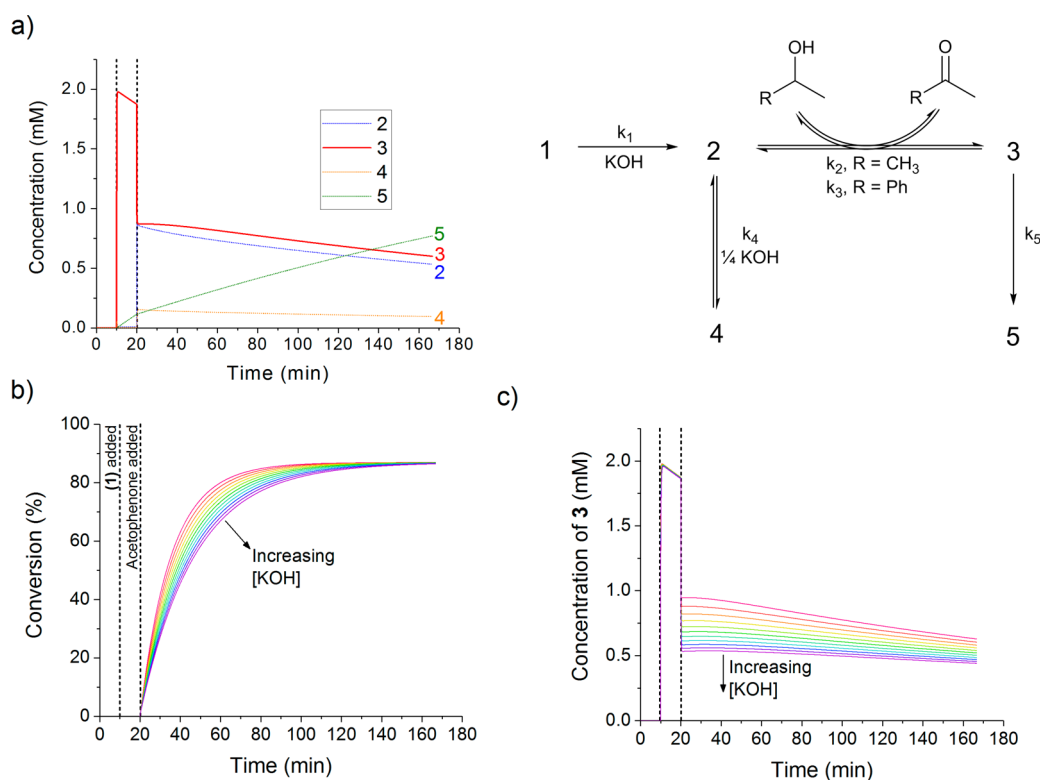
Scheme 3. Expanded Mechanism for Catalytic Transfer Hydrogenation Using 1 Including Base-Induced Formation of off-Cycle Species 4 from 2 and Deactivation of 3 to 5 with the Associated Rate Law
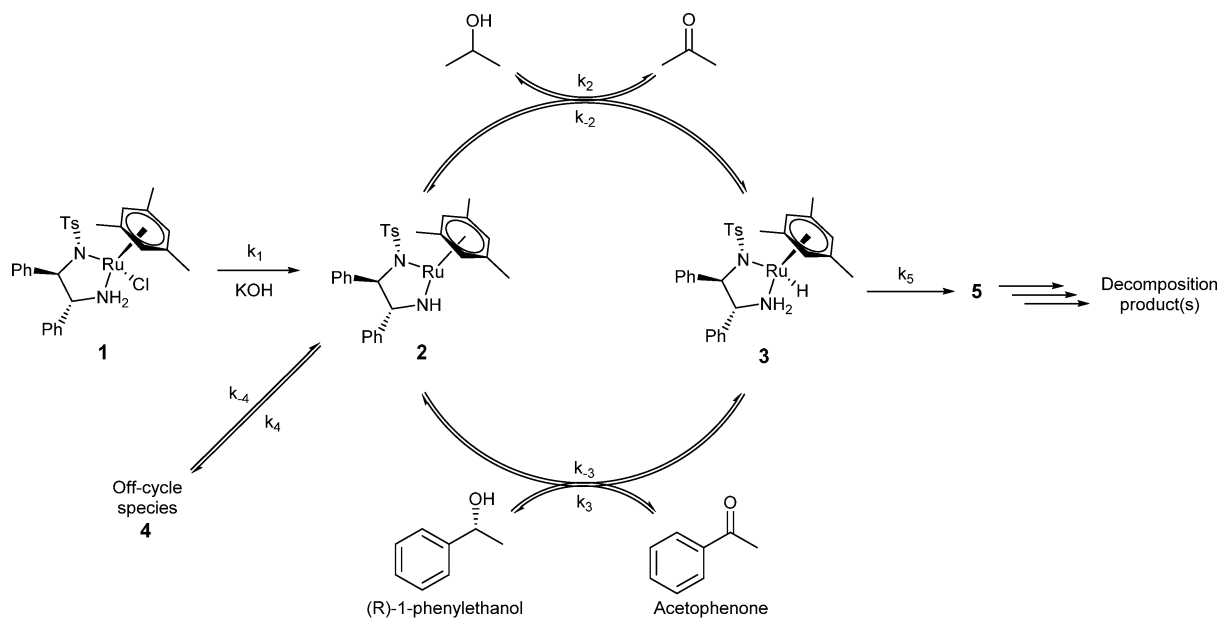
$$rate = (k_3[Acp] - k_{-3}[PE]K_{cat})\left(K_{cat}^{-1} + \frac{k_{-4}}{k_4[KOH]^{0.25}K_{cat} + 1} + 1\right)\left([Ru]_0 \exp\left\{-\left(k_5\left(K_{cat}^{-1} + \frac{k_{-4}}{k_4[KOH]^{0.25}K_{cat} + 1} + 1\right)\right)\right\}\right)$$

$$K_{cat} = \frac{[2]}{[3]} = \frac{k_{-2}[Ac] + k_3[Acp]}{k_2[IPA] + k_{-3}[PE]} = \frac{k_{-2}\chi[Acp]_0 + k_3[Acp]_0(1-\chi)}{k_2[IPA]_0 + k_{-3}\chi[Acp]_0}$$

Figure 11. Simulated reaction kinetics for proposed modification of the catalytic transfer hydrogenation mechanism of **1** (Scheme 3), including the effect of varying KOH concentration on (a) catalyst speciation, (b) reaction progress, and (c) hydride profiles. See Supporting Information for details of simulation, kinetic parameters, and derivation of rate laws.

base added. The instability of **3** that leads to gradual catalyst decomposition is more intriguing, as it appears to be an inherent

feature of the catalyst that limits its effective turnover number and progressively erodes enantioselectivity over time (Figure
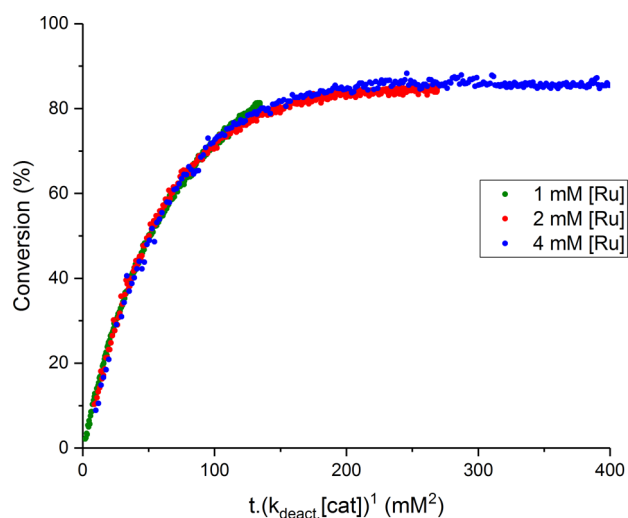
Figure 12. VTNA plot for the catalytic transfer hydrogenation of acetophenone to (*R*)-1-phenylethanol with various amounts of **1**, adjusted for experimentally observed catalyst deactivation (Figure 7) (400 mM acetophenone, 10 mM KOH, 9.5 mL of dry isopropyl alcohol, 20 °C).

Scheme 4. Formation of Base Adduct Complexes 4 from the Unsaturated Intermediate 2 (In-Cycle for Isopropyl Alcohol or 1-Phenylethanol and Off-Cycle for KOH/H₂O)
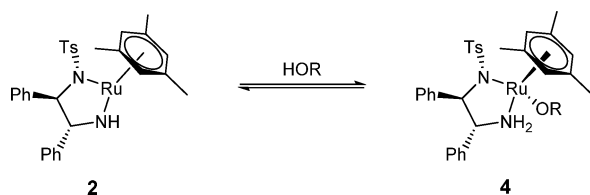

4b). Complete ligand loss and eventual formation of ruthenium black has been observed before in this chemistry;[45] however, as we have found the rate of this multistep degradation pathway to be first-order in **3** (Figure S6), its rate-determining step (as described by k_5) must involve a key transformation of the molecular hydride intermediate.

In a typical ^{1}H FlowNMR experiment carried out under literature conditions, most ligand signals were obscured by dominant solvent, substrate, and product peaks. Various NMR strategies for resolving minor signals underneath dominant peaks exist (including advanced spectral deconvolution,[27,51,52] multiple solvent suppression,[53,54] and 2D experiments with T_1, T_2, or diffusion filtering[55−57]), these may be challenging in cases where multiple, a priori unknown minor signals are to be detected and quantified in the vicinity of much more intense peaks. Chemical modification of the system by way of isotopic labeling is an alternative strategy for discriminating different species or functionalities using different NMR frequencies. In this case, perdeuterated solvent is commercially available, so using this with the standard (i.e., nondeuterated) Noyori catalyst moves these dominant resonances into the ^{2}H domain, allowing multiple catalyst signatures to be resolved in the ^{1}H spectra (Scheme 5).

As mentioned above, deuteration of the solvent entailed a significant primary kinetic isotope effect of $k_H/k_D = 5.85$ on the reaction (Figure S7) proceeding through a series of X-H/D cleavage steps (X = C, O, Ru). Furthermore, rapid exchange of the acetophenone CH₃ protons with deuterium was observed

Scheme 5. Catalytic Asymmetric Transfer Hydrogenation of Acetophenone to (*R*)-1-Phenylethanol with RuCl[(*R,R*)-TsDPEN](mesitylene) (1) in Isopropyl Alcohol-d_8 Solution
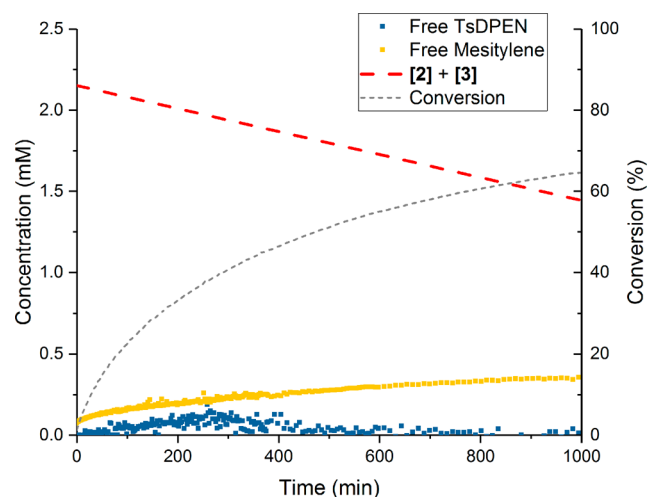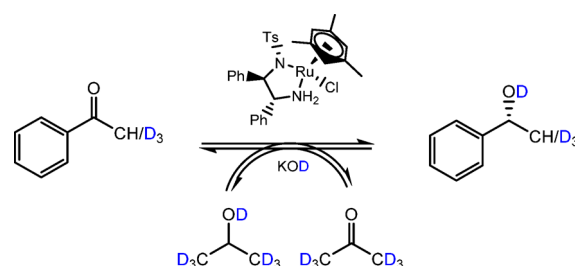

Figure 13. Concentration profile of combined **2** + **3** (determined from TsDPEN C<u>H</u> peaks), free TsDPEN, and free mesitylene during the course of catalytic transfer hydrogenation reaction of acetophenone to (*R*)-1-phenylethanol in flow at 2 mL/min (2 mM **1**, 400 mM acetophenone, 20 mM KOD, 9.5 mL of isopropyl alcohol-d_8, 20 °C, 16 scans, 1.64 s acquisition time, 1 s delay time). Essentially no free TsDPEN signals were observed throughout the reaction; the slight scatter between 100 and 500 min stems from tailing of other resonances into the chemical shift range of free TsDPEN (see Figure S8 for an example spectrum).
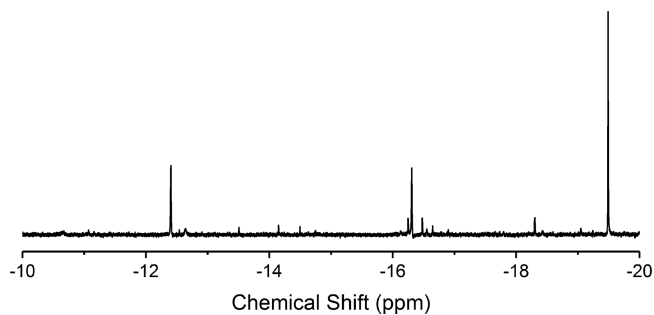
Figure 14. Sample ^{1}H selective excitation NMR spectrum of **1** heated in isopropyl alcohol in the presence of excess KOH for 6 h (due to wide excitation range (10 ppm), signals are nonquantitative; peak intensities of different species observed to vary over time).

under the basic conditions applied (Figure S8), as expected for an enolizable ketone. More importantly, however, interleaving ^{1}H and ^{2}H FlowNMR acquisitions on this partially deuterated system allowed us to follow the fate of the mesitylene and TsDPEN ligands bound to the ruthenium over the course of the reaction. As previously seen from the profiles of **3** using selective

Scheme 6. Proposed Mode of Catalyst Deactivation by Formation of Hydride-Bridged Dimers 5 (Figure 14) from 3 as the First Step Leading to Decomposition into Ru Black (n = 1, 2, 3 with Remaining Coordination Sites Occupied by Solvent)
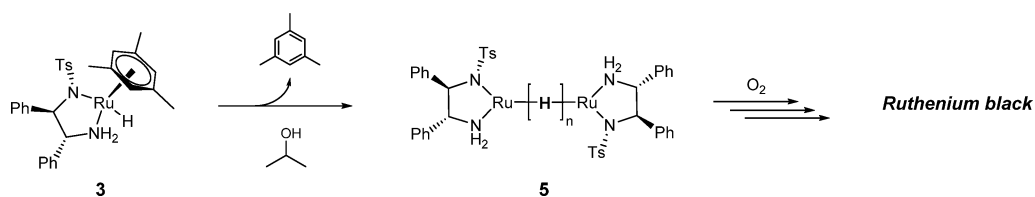
excitation of the hydride signal, the concentrations of both **2** and **3** were observed to decrease over time as the catalysis converged to equilibrium (Figure 13). Whereas virtually all detectable TsDPEN signals originated from metal-bound species, the continuous liberation of mesitylene from the catalyst was clearly observed (as shown by spiking with authentic samples at the end of the reaction).

The formation of free mesitylene kinetically correlated with the onset of catalyst deactivation, showing it to be part of the rate-determining step in k_5. This observation clearly showed loss of the arene ligand to be the Achilles' heel of these widely used (arene)Ru(TsDPEN) transfer hydrogenation catalysts. When **3** was heated or left in isopropyl alcohol solution for prolonged periods of time, additional hydride peaks were observed to form at the expense of **3** in the ^{1}H NMR spectra (Figure 14). Although their multitude and low abundances precluded more comprehensive characterization, their characteristic chemical shift range (−10 to −20 ppm as compared to −5.3 ppm for **3**), and T_1 values (4−5 s as compared to 0.25 s for **3**) are in good agreement with their formulation as hydride-bridged dimers.[58]

We therefore conclude that catalyst deactivation from **3** occurs by way of loss of the mesitylene ligand to form inactive hydride bridged dimeric ruthenium species, which then transform further into ruthenium nanoparticles as the final degradation product (Scheme 6). Although an $\eta^6 L_3$ arene ligand may be expected to be more strongly bound to the metal center than an η^2 LX amino/amido ligand in terms of coordination chemistry principles, the situation is clearly different in catalysis where multiple reagents present in large excess repeatedly push the catalyst through a series of intermediates. Reversible hapticity shifts of the bound arene have been discussed in the context of the mechanism of transfer hydrogenation before (i.e., in the interconversion of **2** and **3**),[41] whereas the TsDPEN ligand is only required to switch between an LX and an $X_2 \eta^2$ coordination mode throughout the cycle, making it more resilient to dissociation than the arene ligand.

Our observation of arene loss leading to catalyst deactivation is consistent with the increased stability reported for Noyori-type Ru catalysts containing an arene ring that is tethered to the chiral TsDPEN ligand,[32,59−62] and similar ligand loss and formation of hydride-bridged dimers have been reported for related iridium-based transfer hydrogenation catalysts.[4,63,64]

CONCLUSIONS

We have shown high-resolution FlowNMR spectroscopy to be a powerful noninvasive tool for studying air-sensitive transition metal catalysis under working conditions in real time. Using variable time normalization analysis, the data are particularly well-suited for reaction progress kinetic analysis as a straightforward way of obtaining relevant kinetic information on the reaction system. Highly enantioselective acetophenone transfer hydrogenation from basic isopropyl alcohol by Noyori's [(mesitylene)(TsDPEN)RuCl] catalyst system has been shown

to follow ideal first-order kinetics up to ∼50% conversion, after which deviations became apparent in the RPKA. By kinetically correlating reaction progress with the concentration of Ru−H intermediate **3** during transfer hydrogenation catalysis initiated by sequential addition of reagents, and comparing it with modeled profiles derived from the rate law of the reaction, we were able to find evidence for two independent catalyst deactivation/inhibition events: deactivation of hydride intermediate **3** caused by gradual loss of the arene ligand and competitive inhibition of unsaturated intermediate **2** by excess base. Inclusion of both pathways into the reaction mechanism resulted in a kinetic model that accurately reproduces all experimental data and accounts for observations of the effect of varying base concentration on conversion. These new mechanistic insights gained into the widely used hydrogen transfer chemistry mediated by (arene)Ru(TsDPEN)-type complexes provide a basis for devising strategies to combat catalyst decomposition, and hopefully stimulate wider use of operando spectroscopy for a better understanding of the dynamic and interlinked processes operational in many other examples of solution phase catalysis.

■ ASSOCIATED CONTENT

ⓢ Supporting Information

The Supporting Information is available free of charge on the ACS Publications website at DOI: 10.1021/acscatal.8b03530.

> Additional experimental data and diagrams; photographs of reaction mixture before and after reaction; details of NMR pulse sequences; calibration methods for selective excitation data; apparatus design, methodology, and synthetic procedures; parameters for kinetic modeling; derivation of rate laws (PDF)

■ AUTHOR INFORMATION

Corresponding Author

*E-mail: u.hintermair@bath.ac.uk.

ORCID ⓘ

Ulrich Hintermair: 0000-0001-6213-378X

Notes

The authors declare the following competing financial interest(s): AC is an employee of Bruker UK Ltd., manufacturer and supplier of NMR hard- and software solutions that have been used in this research. The other authors declare no competing financial interest.

■ ACKNOWLEDGMENTS

■ DEDICATION

Dedicated to Prof. Robert H. Crabtree on the occasion of his 70th birthday.

■ REFERENCES

(1) Trost, B. M. Atom Economy - A Challenge for Organic Synthesis: Homogeneous Catalysis Leads the Way. *Angew. Chem., Int. Ed. Engl.* **1995**, *34*, 259−281.

(2) Crabtree, R. H. *The Organometallic Chemistry of the Transition Metals*, 4th ed.; John Wiley & Sons, Inc.: Hoboken, NJ, 2005; Vol. *1*, pp 235−273.

(3) Kurosawa, H.; Yamamoto, A. *Fundamentals of Molecular Catalysis*, 3rd ed.; Elsevier: Amsterdam, 2003; Vol. *1*.

(4) Crabtree, R. H. Deactivation in homogeneous transition metal catalysis: causes, avoidance, and cure. *Chem. Rev.* **2015**, *115*, 127−150.

(5) Cornils, B.; Herrmann, W. A. *Applied Homogeneous Catalysis with Organometallic Compounds: A Comprehensive Handbook in Three Volumes*, 2nd ed.; Wiley-VCH: Weinheim, 2002; Vol. *1*.

(6) Moser, W. R.; Slocum, D. W. *Homogeneous Transition Metal Catalyzed Reactions*, 1st ed.; American Chemical Society: Washington, D.C., 1992; Vol. *230*.

(7) Mahatthananchai, J.; Dumas, A. M.; Bode, J. W. Catalytic selective synthesis. *Angew. Chem., Int. Ed.* **2012**, *51*, 10954−10990.

(8) Blackmond, D. G. Reaction Progress Kinetic Analysis: A Powerful Methodology for Mechanistic Studies of Complex Catalytic Reactions. *Angew. Chem., Int. Ed.* **2005**, *44*, 4302−4320.

(9) Bures, J. Variable Time Normalization Analysis: General Graphical Elucidation of Reaction Orders from Concentration Profiles. *Angew. Chem., Int. Ed.* **2016**, *55*, 16084−16087.

(10) Blackmond, D. G. Kinetic Profiling of Catalytic Organic Reactions as a Mechanistic Tool. *J. Am. Chem. Soc.* **2015**, *137*, 10852−10866.

(11) Chung, R.; Hein, J. E. The More, The Better: Simultaneous In Situ Reaction Monitoring Provides Rapid Mechanistic and Kinetic Insight. *Top. Catal.* **2017**, *60*, 594−608.

(12) Rabeah, J.; Bentrup, U.; Stober, R.; Bruckner, A. Selective Alcohol Oxidation by a Copper TEMPO Catalyst: Mechanistic Insights by Simultaneously Coupled Operando EPR/UV-Vis/ATR-IR Spectroscopy. *Angew. Chem., Int. Ed.* **2015**, *54*, 11791−11794.

(13) Catalysis as it goes. *Nature Catalysis* **2018**, *1*, 165−166; .

(14) Brinkman, U. A. T. A review of reaction detection in HPLC. *Chromatographia* **1987**, *24*, 190−200.

(15) Cervera-Padrell, A. E.; Nielsen, J. P.; Jønch Pedersen, M.; Müller Christensen, K.; Mortensen, A. R.; Skovby, T.; Dam-Johansen, K.; Kiil, S.; Gernaey, K. V. Monitoring and Control of a Continuous Grignard Reaction for the Synthesis of an Active Pharmaceutical Ingredient Intermediate Using Inline NIR spectroscopy. *Org. Process Res. Dev.* **2012**, *16*, 901−914.

(16) Foley, D. A.; Wang, J.; Maranzano, B.; Zell, M. T.; Marquez, B. L.; Xiang, Y.; Reid, G. L. Online NMR and HPLC as a reaction monitoring platform for pharmaceutical process development. *Anal. Chem.* **2013**, *85*, 8928−8932.

(17) Schafer, W. A.; Hobbs, S.; Rehm, J.; Rakestraw, D. A.; Orella, C.; McLaughlin, M.; Ge, Z.; Welch, C. J. Mobile Tool for HPLC Reaction Monitoring. *Org. Process Res. Dev.* **2007**, *11*, 870−876.

(18) Kumar, P. In *Advanced Gas Chromatography: Progress in Agricultural Biomedical and Industrial Applications*, 1st ed.; Ali Mohd, M., Ed.; InTech, 2012; Vol. *1*, pp 325−342.

(19) Hart, R. J.; Pedge, N. I.; Steven, A. R.; Sutcliffe, K. In situ Monitoring of a Heterogeneous Etherification Reaction Using Quantitative Raman Spectroscopy. *Org. Process Res. Dev.* **2015**, *19*, 196−202.

(20) Hall, A. M. R.; Chouler, J. C.; Codina, A.; Gierth, P. T.; Lowe, J. P.; Hintermair, U. Practical Aspects of Real-time Reaction Monitoring using Multi-nuclear High Resolution FlowNMR Spectroscopy. *Catal. Sci. Technol.* **2016**, *6*, 8406−8417.

(21) Foley, D. A.; Bez, E.; Codina, A.; Colson, K. L.; Fey, M.; Krull, R.; Piroli, D.; Zell, M. T.; Marquez, B. L. NMR flow tube for online NMR reaction monitoring. *Anal. Chem.* **2014**, *86*, 12008−12013.

(22) Foley, D. A.; Dunn, A. L.; Zell, M. T. Reaction monitoring using online vs tube NMR spectroscopy: seriously different results. *Magn. Reson. Chem.* **2016**, *54*, 451−456.

(23) Maiwald, M.; Fischer, H. H.; Kim, Y.-K.; Albert, K.; Hasse, H. Quantitative high-resolution on-line NMR spectroscopy in reaction and process monitoring. *J. Magn. Reson.* **2004**, *166*, 135−146.

(24) Maiwald, M.; Fischer, H. H.; Kim, Y.-K.; Hasse, H. Quantitative on-line high-resolution NMR spectroscopy in process engineering applications. *Anal. Bioanal. Chem.* **2003**, *375*, 1111−1115.

(25) Barrios Sosa, A. C.; Williamson, R. T.; Conway, R.; Shankar, A.; Sumpter, R.; Cleary, T. A Safe and Efficient Synthetic Route to a 2,5-Dimethyl-1-aryl-1H-imidazole Intermediate. *Org. Process Res. Dev.* **2011**, *15*, 449−454.

(26) Blanazs, A.; Bristow, T. W.; Coombes, S. R.; Corry, T.; Nunn, M.; Ray, A. D. Coupling and optimization of online nuclear magnetic resonance spectroscopy and mass spectrometry for process monitoring to cover the broad range of process concentration. *Magn. Reson. Chem.* **2017**, *55*, 274−282.

(27) Zientek, N.; Meyer, K.; Kern, S.; Maiwald, M. Quantitative Online NMR Spectroscopy in a Nutshell. *Chem. Ing. Tech.* **2016**, *88*, 698−709.

(28) Wang, D.; Astruc, D. The golden age of transfer hydrogenation. *Chem. Rev.* **2015**, *115*, 6621−6686.

(29) Baratta, W.; Ballico, M.; Baldino, S.; Chelucci, G.; Herdtweck, E.; Siega, K.; Magnolia, S.; Rigo, P. New Benzo[*h*]quinoline-Based Ligands and their Pincer Ru and Os Complexes for Efficient Catalytic Transfer Hydrogenation of Carbonyl Compounds. *Chem. - Eur. J.* **2008**, *14*, 9148−9160.

(30) Bullock, R. M. Catalytic Ionic Hydrogenations. *Chem. - Eur. J.* **2004**, *10*, 2366−2374.

(31) Eisenstein, O.; Crabtree, R. H. Outer sphere hydrogenation catalysis. *New J. Chem.* **2013**, *37*, 21−27.

(32) Hayes, A. M.; Morris, D. J.; Clarkson, G. J.; Wills, M. A class of ruthenium(II) catalyst for asymmetric transfer hydrogenations of ketones. *J. Am. Chem. Soc.* **2005**, *127*, 7318−7319.

(33) Misal Castro, L. C.; Li, H.; Sortais, J.-B.; Darcel, C. When iron met phosphines: a happy marriage for reduction catalysis. *Green Chem.* **2015**, *17*, 2283−2303.

(34) Noyori, R. Ryoji Noyori - Nobel Lecture: Asymmetric Catalysis: Science and Technology; http://www.nobelprize.org/nobel_prizes/chemistry/laureates/2001/noyori-lecture.html (accessed June 27, 2018).

(35) Noyori, R.; Hashiguchi, S. Asymmetric Transfer Hydrogenation Catalyzed by Chiral Ruthenium Complexes. *Acc. Chem. Res.* **1997**, *30*, 97−102.

(36) Wang, C.; Wu, X.; Xiao, J. Broader, greener, and more efficient: recent advances in asymmetric transfer hydrogenation. *Chem. - Asian J.* **2008**, *3*, 1750−1770.

(37) Hashiguchi, S.; Fujii, A.; Takehara, J.; Ikariya, T.; Noyori, R. Asymmetric Transfer Hydrogenation of Aromatic Ketones Catalyzed by Chiral Ruthenium(II) Complexes. *J. Am. Chem. Soc.* **1995**, *117*, 7562−7563.

(38) Haack, K.-J.; Hashiguchi, S.; Fujii, A.; Ikariya, T.; Noyori, R. The Catalyst Precursor, Catalyst and Intermediate in the Ru(II)-Promoted Asymmetric Hydrogen Transfer between Alcohols and Ketones. *Angew. Chem., Int. Ed. Engl.* **1997**, *36*, 285−288.

(39) Noyori, R. Asymmetric catalysis: Science and opportunities (Nobel lecture). *Angew. Chem., Int. Ed.* **2002**, *41*, 2008−2022.

(40) Vaclavik, J.; Sot, P.; Vilhanova, B.; Pechacek, J.; Kuzma, M.; Kacer, P. Practical aspects and mechanism of asymmetric hydrogenation with chiral half-sandwich complexes. *Molecules* **2013**, *18*, 6804−6828.

(41) Clapham, S. E.; Hadzovic, A.; Morris, R. H. Mechanisms of the H₂-hydrogenation and transfer hydrogenation of polar bonds catalyzed by ruthenium hydride complexes. *Coord. Chem. Rev.* **2004**, *248*, 2201−2237.

(42) Dub, P. A.; Henson, N. J.; Martin, R. L.; Gordon, J. C. Unravelling the mechanism of the asymmetric hydrogenation of acetophenone by [RuX₂(diphosphine)(1,2-diamine)] catalysts. *J. Am. Chem. Soc.* **2014**, *136*, 3505−3521.

(43) Koike, T.; Ikariya, T. Mechanistic Aspects of Formation of Chiral Ruthenium Hydride Complexes from 16-Electron Ruthenium Amide Complexes and Formic Acid: Facile Reversible Decarboxylation and Carboxylation. *Adv. Synth. Catal.* **2004**, *346*, 37−41.

(44) Strotman, N. A.; Baxter, C. A.; Brands, K. M. J.; Cleator, E.; Krska, S. W.; Reamer, R. A.; Wallace, D. J.; Wright, T. J. Reaction Development and Mechanistic Study of a Ruthenium Catalyzed Intramolecular Asymmetric Reductive Amination en Route to the Dual Orexin Inhibitor Suvorexant (MK-4305). *J. Am. Chem. Soc.* **2011**, *133*, 8362−8371.

(45) Toubiana, J.; Medina, L.; Sasson, Y. The Nature of the True Catalyst in Transfer Hydrogenation with Alcohol Donors Using (arene)₂Ru₂Cl₄(II)/TsDPEN Precursor. *Mod. Res. Catal.* **2014**, *3*, 68−88.

(46) Blackmond, D. G.; Ropic, M.; Stefinovic, M. Kinetic Studies of the Asymmetric Transfer Hydrogenation of Imines with Formic Acid Catalyzed by Rh−Diamine Catalysts. *Org. Process Res. Dev.* **2006**, *10*, 457−463.

(47) Bures, J. A Simple Graphical Method to Determine the Order in Catalyst. *Angew. Chem., Int. Ed.* **2016**, *55*, 2028−2031.

(48) Dub, P. A.; Ikariya, T. Quantum chemical calculations with the inclusion of nonspecific and specific solvation: asymmetric transfer hydrogenation with bifunctional ruthenium catalysts. *J. Am. Chem. Soc.* **2013**, *135*, 2604−2619.

(49) Yamakawa, M.; Ito, H.; Noyori, R. The Metal−Ligand Bifunctional Catalysis: A Theoretical Study on the Ruthenium(II)-Catalyzed Hydrogen Transfer between Alcohols and Carbonyl Compounds. *J. Am. Chem. Soc.* **2000**, *122*, 1466−1478.

(50) Wu, X.; Liu, J.; Di Tommaso, D.; Iggo, J. A.; Catlow, C. R. A.; Bacsa, J.; Xiao, J. A Multilateral Mechanistic Study into Asymmetric Transfer Hydrogenation in Water. *Chem. - Eur. J.* **2008**, *14*, 7699−7715.

(51) Zientek, N.; Laurain, C.; Meyer, K.; Paul, A.; Engel, D.; Guthausen, G.; Kraume, M.; Maiwald, M. Automated data evaluation and modelling of simultaneous ¹⁹F-¹H medium-resolution NMR spectra for online reaction monitoring. *Magn. Reson. Chem.* **2016**, *54*, 513−520.

(52) Silva Elipe, M. V.; Milburn, R. R. Monitoring chemical reactions by low-field benchtop NMR at 45 MHz: pros and cons. *Magn. Reson. Chem.* **2016**, *54*, 437−443.

(53) Smallcombe, S. H.; Patt, S. L.; Keifer, P. A. WET Solvent Suppression and Its Applications to LC NMR and High-Resolution NMR Spectroscopy. *J. Magn. Reson., Ser. A* **1995**, *117*, 295−303.

(54) Zheng, G.; Price, W. S. Solvent signal suppression in NMR. *Prog. Nucl. Magn. Reson. Spectrosc.* **2010**, *56*, 267−288.

(55) Tang, H.; Wang, Y.; Nicholson, J. K.; Lindon, J. C. Use of relaxation-edited one-dimensional and two dimensional nuclear magnetic resonance spectroscopy to improve detection of small metabolites in blood plasma. *Anal. Biochem.* **2004**, *325*, 260−272.

(56) Asada, M.; Nemoto, T.; Mimura, H.; Sako, K. Advanced New Relaxation Filter-Selective Signal Excitation Methods for ¹³C Solid-State Nuclear Magnetic Resonance. *Anal. Chem.* **2014**, *86*, 10091−10098.

(57) Esturau, N.; Espinosa, J. F. Optimization of Diffusion-Filtered NMR Experiments for Selective Suppression of Residual Non-deuterated Solvent and Water Signals from ¹H NMR Spectra of Organic Compounds. *J. Org. Chem.* **2006**, *71*, 4103−4110.

(58) Jahncke, M.; Meister, G.; Rheinwald, G.; Stoeckli-Evans, H.; Süss-Fink, G. Dinuclear (Arene)ruthenium Hydrido Complexes: Synthesis, Structure, and Fluxionality of (C₆Me₆)₂Ru₂H₃(BH₄). *Organometallics* **1997**, *16*, 1137−1143.

(59) Cheung, F. K.; Hayes, A. M.; Hannedouche, J.; Yim, A. S.; Wills, M. ″Tethered″ Ru(II) catalysts for asymmetric transfer hydrogenation of ketones. *J. Org. Chem.* **2005**, *70*, 3188−3197.

(60) Soni, R.; Hall, T. H.; Mitchell, B. P.; Owen, M. R.; Wills, M. Asymmetric Reduction of Electron-Rich Ketones with Tethered Ru(II)/TsDPEN Catalysts Using Formic Acid/Triethylamine or Aqueous Sodium Formate. *J. Org. Chem.* **2015**, *80*, 6784−93.

(61) Touge, T.; Hakamata, T.; Nara, H.; Kobayashi, T.; Sayo, N.; Saito, T.; Kayaki, Y.; Ikariya, T. Oxo-Tethered Ruthenium(II) Complex as a Bifunctional Catalyst for Asymmetric Transfer Hydrogenation and H₂ Hydrogenation. *J. Am. Chem. Soc.* **2011**, *133*, 14960−14963.

(62) Nedden, H. G.; Zanotti-Gerosa, A.; Wills, M. The Development of Phosphine-Free 'Tethered' Ruthenium(II) Catalysts for the Asymmetric Reduction of Ketones and Imines. *Chem. Rec.* **2016**, *16*, 2623−2643.

(63) Letko, C. S.; Heiden, Z. M.; Rauchfuss, T. B. Activation and Deactivation of Cp*Ir(TsDPEN) Hydrogenation Catalysts in Water. *Eur. J. Inorg. Chem.* **2009**, *2009*, 4927−4930.

(64) Campos, J.; Hintermair, U.; Brewster, T. P.; Takase, M. K.; Crabtree, R. H. Catalyst Activation by Loss of Cyclopentadienyl Ligands in Hydrogen Transfer Catalysis with Cp*IrIII Complexes. *ACS Catal.* **2014**, *4*, 973−985.